The lightning performance of a 400 kV composite pylon with cable as down-lead

Kai Yin, Filipe Miguel Faria da Silva, Claus Leth Bak, Hanchi Zhang

Abstract—**This paper investigates the effect of the impulse corona inside the cross-arm on the lightning performance of a Y-shaped composite pylon with a cable as an internal down-lead through the hollow cross-arm. First, the electromagnetic transient model for the down-lead system of the composite pylon is built. The simplified steps for calculating the surge impedance of the cable down-lead are given. In addition, the mutual coupling between two down-leads is considered. Through a laboratory test on coaxial cylinders resembling the structure of the cable and cross-arm, the dynamic capacitance of the corona on the surface of the cable is obtained and included in the electromagnetic transient model. Then, the effect of the corona on the traveling waveform and mutual capacitance is discussed. Furthermore, the influences of the ground electrode length and the phase voltage on lightning performance are also studied. Finally, the backflash rates of the composite pylon with cable as down-lead are calculated. The results show that the impulse corona has a limited impact on the critical current, and the composite pylon with cable as down-lead shows a promising lightning performance.**

Keywords: **BFR, Cable, Composite pylon, Down-lead, Impulse corona, Lightning performance.**

I. INTRODUCTION

IN recent years, composite pylon has attracted wide attention in transmission construction due to its high reliability, environmental friendliness [1], and low production and maintenance cost [2]. A possible design is the 400 kV composite pylon with a steel mast and two hollow cross-arms and forming a 'Y' pattern shown in Fig. 1. The pylon has a compact configuration, and each one-piece hollow cross-arm carries three phase conductors and one shield wire. It possesses high electrical insulation, thermal stability, and mechanical properties, and requires less right-of-way [3]. In addition, the theoretical calculation based on the electrogeometric model and experimental test proved that this kind of pylon has a very low shielding failure rate of 0.0008 flashes/year for 100 km lines [1]. With these attractive advantages, this pylon has a great application prospect in future overhead lines [3].

Different from the traditional tower whose metal cross-arm and lattice body are conductive to the lightning current, the composite pylon primarily made of Fiber Reinforced Plastic cannot provide zero potential to the shield wire and a grounding path for the lightning stroke. Therefore, a down-lead system should be specially designed for this type of composite tower to reduce the overvoltage level and keep the transmission line operating safely in the event of a lightning strike [4]. Here, a cable passing through the hollow cross-arm and connecting with the metallic mast is proposed as the down-lead [4]. However, to date, there is a lacking practical cases of a cable as a down-lead in HV towers. Research on the lightning performance of a composite pylon with a cable as a down-lead is absent.

Fig. 1. The concept appearance of the Y-shaped pylon used for 400 kV transmission lines.

Of particular concern is that for this composite pylon, the cable as down-lead inside the cross-arm has a small radius, and impulse corona is inevitable when the pylon is struck by lightning. To investigate the lightning behavior of the pylon, the corona effect on the cable down-lead should be taken into account. A large amount of research has been previously done to study the characteristics of the corona generated on metal cylinders [5]-[7]. However, in this research, the corona emanates from an insulation material cylinder rather than a steel one, which may lead to different inception properties [8]. The previous research reported that the corona can affect the capacitance of the metal conductors and whether the effect of the impulse corona on a cable's dynamic capacitance is the same as the effect on a bare conductor has not been reported yet. In addition, the previous research mainly focused on the influence of the corona on the transverse propagating surge [5]-[9], while the surge traveling along the down-lead is vertical. How the corona affects the surge traveling process and the lightning overvoltage is unclear. Furthermore, the compact pylon has a much shorter phase to down-lead distance, the

K. Yin is with Energy Department, Aalborg University, Aalborg 9220, Denmark. (e-mail: shenyingkaixuan@163.com).

F. M. F. da Silva is with Energy Department, Aalborg University, Aalborg 9220, Denmark. (e-mail: ffs@energy.aau.dk).

C. L. Bak is with Energy Department, Aalborg University, Aalborg 9220, Denmark. (e-mail: kyi@energy.aau.dk).

Hanchi Zhang is with Energy Department, Aalborg University, Aalborg 9220, Denmark. (e-mail: hazh@energy.aau.dk).

impact of the corona on the mutual coupling and the parasitic capacitance should also be investigated [10].

In order to estimate the lightning performance of the Y-shaped composite pylon and judge whether the cable as a down-lead is a feasible grounding strategy for this novel pylon, we investigate the dynamic corona characteristics on the cable surface and its impact on the lightning performance through electromagnetic transient simulations and laboratory experiments [11]. In Section II, the pylon configuration and the electromagnetic modeling process of the pylon are exhibited. We derive the surge impedance formula of the inclined down-lead and propose a simplified form to facilitate the calculation. Then, we use two coaxial insulation cylinders to resemble the cross-arm structure within a cable. Based on this scale model, the corona characteristics are obtained by experiments, and this part is shown in Section III. Finally, the corona effect of the cable on the critical current I_c of the pylon is analyzed in Section IV.

II. PSCAD MODELING FOR DOWN-LEAD SYSTEM

The 'Y' composite pylon is composed of two Fiber Reinforced Plastic cross-arm tubes and a steel mast. A single cross-arm is 12 meters long, and the height of the pylon mast is 16.5 m [12]. The cross-arm and mast form an inclined angle of 120°. Each cross-arm carries one shield wire and three-phase conductors. The phase-to-phase clearance is 3.6 m and the phase-to-earth distance is 2.8 m [13]. Twin duplex conductors are used as phase conductors with a spacing of 0.3 m, which are fixed by alumina clamps [14]. Double-grading rings are installed on the two sides of the phase clamps [15]. The cable with a constant core radius of 1.75 cm and a 2.6 cm insulation layer thickness is employed as the down-lead. Based on these parameters, the electromagnetic transient model is built in PSCAD/EMTDC software.

A. Surge Impedance of Inclined Down-lead

To build the equivalent circuit of the down-lead system, the surge impedance should be determined, which is mainly associated with the capacitance and inductance of the cable down-lead. Due to the thin cable insulation layer and cross-arm shell, the dielectric impact can be neglected. Referring to the multistory model [16] and employing the image method [17], the down-lead can be divided into four parts (Fig. 2(a)), and the capacitance and inductance of each part are delivered in integral form:

$$L_i = \frac{\mu_0 l}{2\pi} \int_i^{i+1} \ln\left[\frac{2(H+x\tan\theta)}{r/\cos\theta} - 1\right] dx \tag{1}$$

$$C_i = \frac{2\pi\varepsilon_0 l}{\int_i^{i+1} \ln\left[\frac{2(H+x\tan\theta)}{r/\cos\theta} - 1\right] dx} \tag{2}$$

Where ε_0 and μ_0 are the vacuum permittivity and permeability, and r is the radius of the cable core. l is the length of the cable segment. H is the height of the bottom point of the cross-arm. The surge impedance Z_i (i=1, 2, 3, 4) of each cable segment is

$$Z_i = \sqrt{\frac{L_i}{C_i}} \tag{3}$$

The height component $2(H+x\tan\theta)$ is far greater than $r/\cos\theta$, Meanwhile, the integral term $2(H+x\tan\theta)$ can be replaced by the mean height of the cable segment h_i (i=1 to 4), and the integral component in equations (1) and (2) can be simplified as:

$$\int_i^{i+1} \ln(2H+2x\tan\theta)dx \approx \Delta x \ln(2h_i) \tag{4}$$

$$\int_i^{i+1} \ln\left[\frac{2(H+x\tan\theta)}{r/\cos\theta} - 1\right]dx = \ln\left(\frac{2h_i}{r}\right)\Delta x \tag{5}$$

In other words, the position and configuration of the cable down-lead can be simplified by four segments placed horizontally as shown in Fig. 2(b). The surge impedance of the cable segments can be treated as horizontal metal parts [18].

$$Z_i = \frac{1}{2\pi}\sqrt{\frac{\mu_0}{\varepsilon_0}}\ln\left(\frac{2h_i}{r}\right) = 60\ln\left(\frac{2h_i}{r}\right) \tag{6}$$

Furthermore, the comparison of results calculated by integral formulas (1)-(3) and simplified formula (6) is performed and exhibited in Table I. The results show that the difference between values derived from the two approaches is no more than 2.02 %, indicating that equation (6) has high accuracy. In addition, this approximation makes the separated down-lead segments to be at the same height inside two cross-arms and paralleled, which is convenient to calculate the mutual capacitance and inductance (in Section II B). Thus, the simplified multistory down-lead model is employed to establish the equivalent circuit in PSCAD/EMTDC.
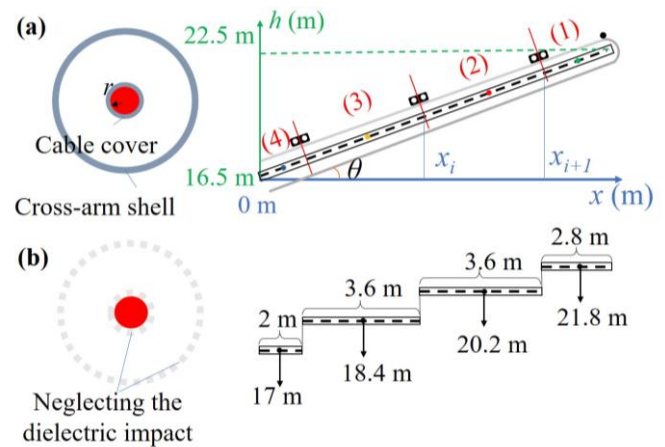

Fig. 2. (a) The schematic of the cross-section of the cross-arm, and down-lead divided into 4 parts from the lateral view. (b) The corresponding simplified down-lead model.

TABLE I
THE COMPARISON OF THE DOWN-LEAD IMPEDANCE RESULTS CALCULATED BY INTEGRAL FORMULAS AND SIMPLIFIED FORMULAS

Z_i of cable segment	i=1	i=2	i=3	i=4
Integral formulas (Ω)	460.25	455.67	450.07	445.34
Simplified formula (Ω)	469.23	464.66	459.06	454.31
Difference (%)	1.95	1.97	2.00	2.02

For the pylon mast with a radius r of 1.5 m, its surge impedance is calculated by [18]

$$Z_m = 60\left[\ln(\frac{2\sqrt{2}\,H}{r}) - 1\right] \quad (7)$$

B. Mutual coupling between two cable down-leads

There is no connection between the two down-lead segments inside the cross-arms. Therefore, when a lightning current passes through one cable, there is the induced voltage in the other one due to the mutual coupling, which can be accounted for by the mutual capacitance and inductance matrices. Based on the simplified down-lead model in Fig. 3(a) and a lossy ground, the shunt capacitance matrix C_P of cable segments i and j can be deduced by the image method [19].

$$C_p = \begin{bmatrix} C_{ii} & C_{ij} \\ C_{ji} & C_{jj} \end{bmatrix} \quad (8)$$

The component C_{ii}/C_{jj} and C_{ij} $(i \neq j)$ in the C_p matrix are given by:

$$C_{ii} = \frac{2\pi\varepsilon_0 l}{\ln\dfrac{2h_i}{r}} \quad (9)$$

$$C_{ij} = \frac{2\pi\varepsilon_0 l \ln\left[\sqrt{\left(\dfrac{2h_i}{d_{ij}}\right)^2 + 1}\right]}{\ln\left[\dfrac{2h_i}{r}\sqrt{\left(\dfrac{2h_i}{d_{ij}}\right)^2 + 1}\right]\ln\left[\dfrac{2h_i}{r}\left(\sqrt{\left(\dfrac{2h_i}{d_{ij}}\right)^2 + 1}\right)^{-1}\right]} \quad (10)$$

For the shunt impedance matrix of the cable down-leads, the earth return path should be considered. As illustrated in Fig. 3(b), Dubanton suggested putting a thin line beneath the ground with a skin depth p, and the complex image method is used to solve this issue [20], and the appropriate impedance matrix between down-lead segment i and j can be represented as

$$Z_I = \begin{bmatrix} Z_{ii} & Z_{ij} \\ Z_{ji} & Z_{jj} \end{bmatrix} = \frac{j\omega\mu_0}{2\pi}\begin{bmatrix} \ln\dfrac{2(h_i+p)}{r} & \ln\dfrac{D_p}{d_{ij}} \\[2mm] \ln\dfrac{D_p}{d_{ji}} & \ln\dfrac{2(h_j+p)}{r} \end{bmatrix} \quad (11)$$

Where p is related to frequency ω, the ground conductivity (S/m) σ and soil permeability μ [20]:

$$p = \frac{1}{\sqrt{j\omega\mu\sigma}} \quad (12)$$
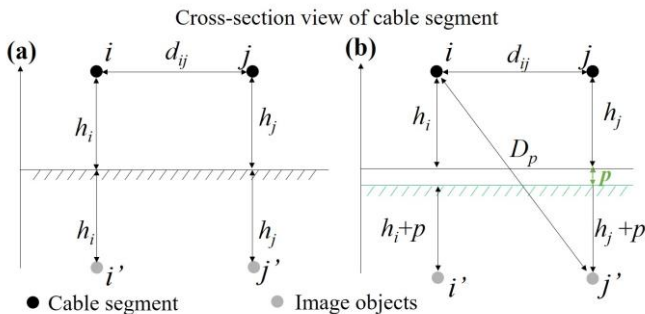
Cross-section view of cable segment

Fig. 3. Geometry of two horizontally placed cable segments in different cross-arms with the application of (a) image method and (b) complex image method.

C. Ground model

A concentrated rod is buried in the uniform soil and installed at the bottom of the pylon mast as the ground electrode for this composite pylon. The total length of the rod is 12 m, and the soil resistivity and relative permittivity are characterized by 100 $\Omega{\cdot}m$ and 10, respectively. In this research, a full-wave electromagnetic field approach is used to get the frequency dependence modeling of the ground [21]. First, the electrode rod is thought of as divided into some segments. Then, the electromagnetic field equations between segments are represented in matrix form. The grounding system admittance matrix is attained by the domain numerical solution of Maxwell's equations based on the method of moment and can be formulated in the form of state-space equations. Finally, the ground dynamic behavior is obtained as shown in Fig. 4. The impedance amplitude and phase angle data are listed in a txt file, and then the file can be input in the FDNE block as the ground equivalent model in PSCAD [22], [23].
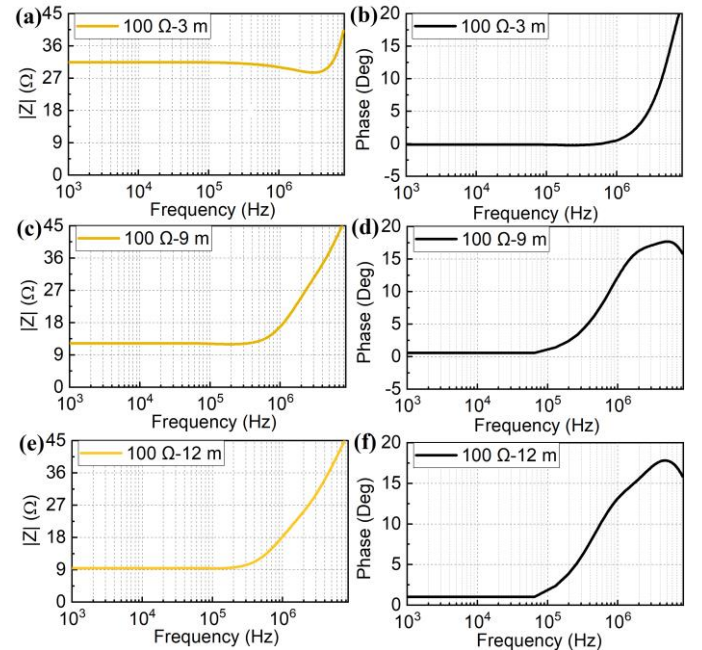
Fig. 4. The harmonic ground impedance of (a) absolute value and (b) phase angle versus frequency.

D. Lightning model

The lightning source is composed of an ideal impulse current source in parallel with a lightning channel impedance. CIGRE lightning waveforms with front time (T_f) of 3.83 μs, tail time (T_t) of 77.5 μs, and amplitude in the range of 0 to 200 kA are employed to attain the critical current through PSCAD simulation. The channel impedance is given as 1000 Ω [17].

E. The criterion of cross-arm flashover

The physical process of the flashover on the cross-arm between the shield wire and the phase conductor can be characterized by Leader Propagation Model. The leader develops in the gap under external stress voltage $u(t)$ as follows:

$$\frac{dx}{dt} = ku(t)\left(\frac{u(t)}{D - h_f - x} - E_0\right) \quad (13)$$

$$h_f = 3.89 / \left(1 + \frac{3.89}{D}\right) \qquad (14)$$

Where x is the length of the leader, D is the phase-to-earth clearance of 2.8 m in this case, E_0 is the leader inception electric field, and k is a coefficient related to the leader propagation velocity. Due to the presence of the grading rings between the shield wire and the upper phase wire, the back-flashover can be regarded as a long gap discharge in the air. Considering the lightning polarity is negative, k and E_0 are set to 1.0×10^{-6} m^2/V^2/s and 670 kV/m according to CIGRE WG C4.23 [24].

The schematic of the equivalent circuit of the pylon down-lead system and the layout of the down-lead model in PSCAD are depicted in Fig. 5.
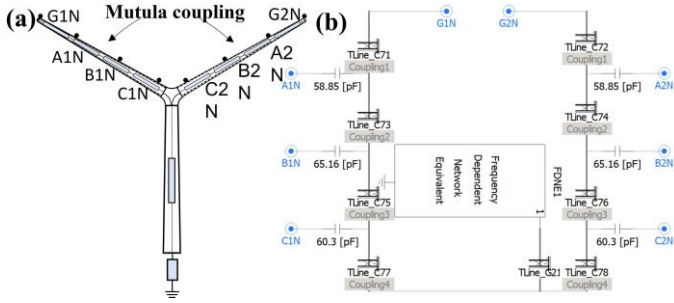

Fig. 5. (a) The schematic of the equivalent circuit. Where GiN, AiN, BiN, and CiN (i=1, 2) refer to shield wires, upper phase, middle phase, and lower phase conductors, respectively. (b) The model of the down-lead system in PSCAD.

III. MODELING OF CORONA

Lightning stroke conducting through the down-lead will emanate a streamer outward along the direction perpendicular to the surface of the cable, which can be regarded as the extension of the down-lead radius and directly affects the capacitance of the down-lead. However, the cable core radius is a fixed value of 1.75 cm, and the presence of the streamer does not change the permeability of the surrounding space. Therefore, the inductance of the down-lead remains constant [18]. In this section, the dynamic capacitance of the cable down-lead with corona is studied and the corresponding equivalent model is built in PSCAD.

A. Corona inception voltage

To obtain the corona inception voltage, the corona inception electric field on the cable surface should be determined. According to our previous research, the corona inception electric gradient E_c as a function of the cylinder radius on the insulation material surface has the almost same pattern as the E_c-radius curve on a metal cylinder **Error! Reference source not found.**. For a cable with a 4.35 cm radius, the corona inception electric field is 26.15 kV/cm **Error! Reference source not found.**. For coaxial cylinder structure, the corona inception voltage in standard atmospheric pressure conditions follows this equation [26]:

$$U_i = a E_c \ln \frac{d}{a} \qquad (15)$$

Where a is the radius of the cable down-lead in cm, and d is the distance between the cable and phase conductor. The calculated corona inception voltage U_i is about 500 kV.

B. Corona effect on capacitance

Normally, the dynamic capacitance of a single conductor can be estimated from the charge-voltage (Q-U) curve [18]. We established an experimental setup to get the Q-U characteristics of the cable. Due to the cable passing through the cross-arm being a coaxial cylinder structure, the dynamic characteristics of the down-lead capacitance can be studied by experiments on a pair of coaxial cylinders. The experimental setup is depicted in Fig. 6. The voltage source can generate an impulse voltage from 0 to 30 kV with 5-15 kHz to simulate the high-frequency components of the lightning waveform. The two insulation cylinders with central axes coinciding form the coaxial cylinders. The radii of the large and small cylinders are 37.5 mm (R_1) and 20 mm (r_1), respectively. Where the external surface of the large cylinder and the inner surface of the small cylinder are taped with copper coils. The source directly connects with the inner surface of the small cylinder. The outer surface of the large cylinder is grounded through a capacitor C_m, which is used to test the charge Q through the coaxial cylinders, which is attained as (16).

$$Q = C_m \times V \qquad (16)$$

Where V is the voltage stressed on C_m. The voltage waveforms on the coaxial cylinders and C_m are shown in Fig. 7. Since the capacitance is dQ/dU, according to the change of the curve slope, the capacitance of coaxial cylinders can be divided into three stages. Stage 1 denotes the voltage increasing from 0 to corona inception voltage U_i. Then continuously increasing the voltage until the crest value U_{crest}, the corona appears, and the capacitance increases, which is called stage 2. When the voltage falls from the crest value to zero, the curve slope returns to the initial state, and this period is stage 3. For stages 1 and 3, the capacitance value is the natural capacitance of the cable down-lead regardless of the applied voltage amplitude, and it can be given as

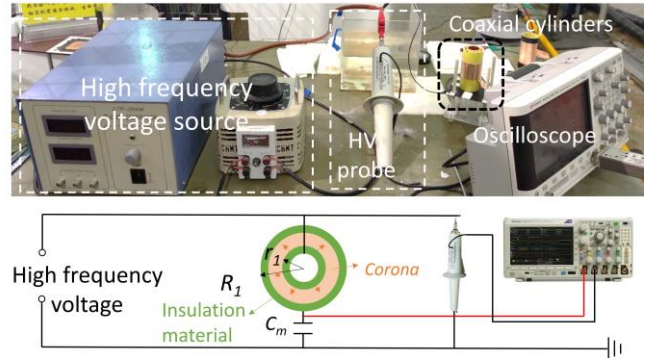$$C_i = \frac{2\pi\varepsilon_0 l}{\ln \frac{2h_i}{a}} \qquad (17)$$

Fig. 6. The photo of the platform to test the corona capacitance and the schematic of the equivalent circuit.

For stage 2, when the applied voltage increases from the inception voltage of 23.9 kV to 26 kV, the dQ/dU (dotted line slope) increases gradually as shown in Fig. 7(b). The Q-U curve of the cable down-lead capacitance is similar to that of the conductor. The corresponding dynamic capacitance can be obtained by referring to the Grey model [27]:

$$C_i = \frac{2\pi\varepsilon_0 l}{\ln\frac{2h_i}{a}}\eta\left(U/U_i\right)^{\eta-1} \quad (18)$$

Where coefficient η is given by $1.121+6.8a$ for negative polarity [27]. However, when the applied voltage is above 26 kV (Fig. 7(b)), the dQ/dU is unchanged, revealing that there is a limit value of the capacitance due to the presence of the larger cylinder. Assuming the cross-arm is a uniform cylinder tube with a radius of 0.3 m. For the cable down-lead, the maximum capacitance is

$$C_n = \frac{2\pi\varepsilon_0 l}{\ln\frac{2h_i}{b}} \quad (19)$$

Where b is the radius of the cross-arm. The corresponding critical voltage for C_i reaching up to C_n is U_t. Thus, C_i in stage 2 can be expressed as a piecewise function:

$$C_i = \begin{cases} \frac{2\pi\varepsilon_0 l}{\ln\frac{2h_i}{a}}\eta\left(\frac{U}{U_i}\right)^{\eta-1}, & U_i \leq U \leq U_t \\ C_n, & U_t \leq U \leq U_{crest} \end{cases} \quad (20)$$

By calculation, U_t is about 574 kV. The lightning current I_i which can make the cable surface voltage reach U_t is displayed in Table II. It can be found that the I_i is far lower than the critical current (I_c should be higher than 100 kA for 400 kV pylon) [17], which means the corona will fill the cross-arm and reach its limited value before the flashover occurrence. To facilitate the modeling of the cable down-lead, the capacitance in stage 2 can be simplified to (21).

$$C_i = C_n, \quad U_i \leq U \leq U_{crest} \quad (21)$$

TABLE II
THE LIGHTNING CURRENT I_i WITH DIFFERENT GROUND ROD LENGTHS

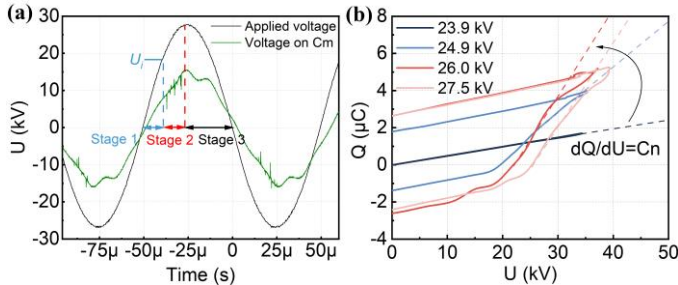| Ground rod length	3 m	9 m	12 m
I_i	29.2 kA	37.5 kA	38.6 kA

Fig. 7. (a) The oscillograms of the stressed voltage on the coaxial cylinders and the capacitor C_m. (b) The Q-U curve with different applied voltages.

IV. CORONA EFFECT ON LIGHTNING PERFORMANCE

A. Corona effect on traveling waves

With the corona expansion from the cable surface to filling the cross-arm, the self-capacitance value of the down-lead segment 1 changes as shown in Fig. 8(a). Meanwhile, the surge impedance and the wave traveling velocity will be influenced simultaneously as depicted in Fig. 8(b). With the corona considered, the surge impedance largely decreases from 440 Ω

to 374 Ω, while the surge propagation velocity decreases from 2.82×10^8 m/s to 2.39×10^8 m/s.

The measured voltage in the middle position of the cable (U_{mR}) shows that a slight decrease in the crest voltage and a 4.8 nanosecond lag of the crest point are observed when compared with a simulation not considering the corona effect (Fig. 9). It can be inferred that the reduction in crest voltage results from the decrease of the surge impedance, and the delayed crest point is owing to the decrease of the propagation velocity.

The critical currents with and without the corona effect have been calculated. In fact, the corona affects the self-impedance and mutual coupling simultaneously. To better assess how the corona affects lightning performance, the corona effects on these two factors are separately considered. First, keeping the mutual coupling setting unchanged, the I_c obtained by simulation is the same value of 176.4 kA whether the corona effect is considered or not. It can be attributed to the conflicting effects of the slow propagation velocity and the decrease of the surge impedance on the lightning performance. The corona emanated from the cable down-lead diverts a fraction of the surge but hinders the conduction capacity of the down-lead for lightning current, and the two effects offset each other and have an overall net effect on the overvoltages. In essence, the electromagnetic energy of lightning current is redistributed in the capacitive form due to the corona. Meanwhile, the instantaneous corona energy loss is insignificant compared with the lightning energy, and the efficiency of the conducting capacity of the down-lead is unchangeable. Thus, it results in that the presence of the corona has no impact on the lightning performance.
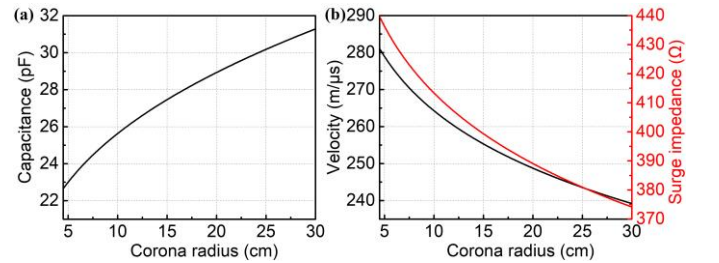
Fig. 8. (a) The variation of the capacitance of the down-lead segment 1 along with the radius expression due to the corona. (b) The surge propagation velocity and the surge impedance of the down-lead segment 1 with different corona radii.
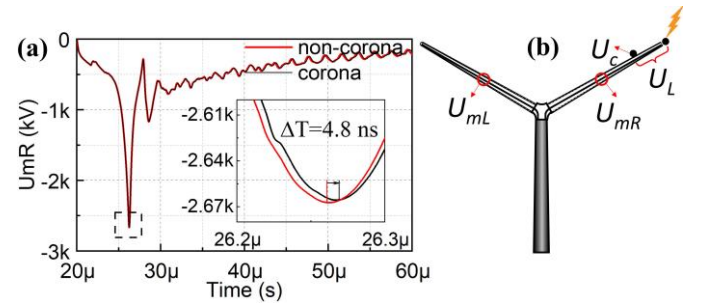
Fig. 9. (a) The voltage waveform in the middle position of the cable down-lead with and without the corona effect. (b) The voltages of interest on different positions of the composite pylon.

B. Corona effect on mutual coupling

The corona effect on the mutual coupling is studied in this

section. Since the mutual inductance between two down-lead segments is uninfluenced by corona, only mutual capacitance needs to be revised according to (8)-(10).

The contrast values of the mutual capacitances between cable segments are listed in Table III. The mutual capacitances are updated in the PSCAD program setting.

TABLE III
THE MUTUAL CAPACITANCE BETWEEN TWO DOWN-LEAD SEGMENTS

C_{ij} $(i=j)$	$i=1$	$i=2$	$i=3$	$i=4$
Non-corona	3.147 pF	52.91 pF	8.201 pF	9.334 pF
Corona	6.170 pF	10.60 pF	17.30 pF	24.54 pF

The expansion of the corona around the cable down-lead will lead to the variation of capacitances between phase voltage and down-lead segments, referred to as the intersection capacitance in this paper. To obtain the intersection capacitance, the full-scale 'Y' composite pylon is built in COMSOL and the line voltages of three phases are set to 420 kV (1.05 p.u.) with 120° phase difference, and the cable down-lead is given a zero potential and the floating potential is set on other metal components. The pylon model is surrounded by air, and the infinite element domain is set for the air boundary. The potential and electric field intensity is attained through the solution of Maxwell equations. Assuming the medium is isotropic and charge-free in the interface, the equation of the electric-field distribution for the individual region in Cartesian coordinates follows the Laplace equation [25]:

$$\frac{\partial^2 \varphi}{\partial x^2} + \frac{\partial^2 \varphi}{\partial y^2} + \frac{\partial^2 \varphi}{\partial z^2} = 0 \tag{22}$$

The potential distribution is calculated (Fig. 10) and intersection capacitance is attained through the Maxwell Matrix (shown in Table IV) [17]. The presence of the corona has led to a three-fold increase in the intersection capacitance values.
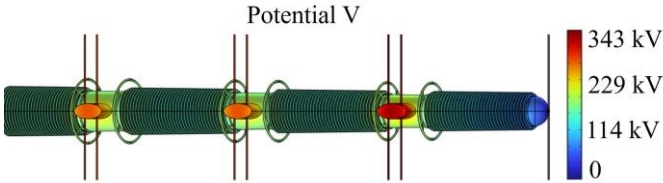
Potential V

343 kV
229 kV
114 kV
0

Fig. 10. The volume potential distribution of the cross-arm.

TABLE IV
THE CAPACITANCE BETWEEN CABLE DOWN-LEAD AND PHASE CONDUCTORS

Parasitic capacitance	Upper phase to cable down-lead	Middle phase to cable down-lead	Lower phase to cable down-lead
Non-corona	58.85 pF	65.16 pF	60.30 pF
Corona	143.86 pF	155.45 pF	147.00 pF

The lightning performance of the pylon with and without the corona effect is simulated. Assuming the lightning strikes at the zero-crossing moment of the upper phase voltage, the critical current (I_c) and overvoltage that appeared at different positions of the pylon are exhibited in Table V. As illustrated in Fig. 9(b), U_{mL} is the voltage measured at the middle of the cable down-lead not struck by lightning, U_c is the upper phase potential, and U_L is the voltage difference between the shield wire and upper phase voltage. Considering the mutual coupling between two

down-leads, I_c increases from 176.4 kA to 177.7 kA with a ground rod of 12 m. The influence of the impulse corona on lightning performance is primarily achieved through the change of mutual capacitances and intersection capacitance. The energy of the lightning current will be transferred to another cable down-lead through the enhanced electromagnetic interaction between them, thus, the overvoltage degree of U_{mL} and U_c is increased. However, the influence of the corona is limited, which can be attributed to the restricted corona expansion by the cross-arm shell. Another reason is that the average distance between two down-leads is relatively long (10.39 m).

TABLE V
I_c AND OVERVOLTAGE ON DIFFERENT POSITIONS OF THE Y-SHAPED PYLON

	Rod length	I_c (kA)	U_{mL} (kV)	U_c (kV)	U_L (kV)
Non-corona	3 m	126.7	-2931.5	-1130.2	2762.5
Corona		127.6	-2980.3	-1192.4	2713.5
Non-corona	9 m	168.9	-2782.2	-1163.5	3045.0
Corona		170.1	-2806.9	-1235.4	2991.1
Non-corona	12 m	176.4	-2577.0	-1165.4	3089.2
Corona		177.7	-2750.6	-1240.4	3032.4

C. Influence of phase voltage

For a transmission line with a voltage above 220 kV, the effect of the phase voltage on the lightning performance should be taken into consideration [28]. The relationship between the upper phase voltage and I_c for 'Y' composite pylon with different ground electrode lengths is illustrated in Fig. 11(a). As the phase voltage increases from negative crest to positive crest, I_c values increase almost linearly. To quantify the variations of the critical current, the I_c-phase angle curves with and without the corona effect are plotted in Fig. 11(b). When upper phase voltage U_p follows this equation:

$$U_p = \frac{420\sqrt{2}}{\sqrt{3}} \cos(x+90) \tag{23}$$

Where x is the phase angle. The I_c - x curves also display a sine shape, which can be fitted as:

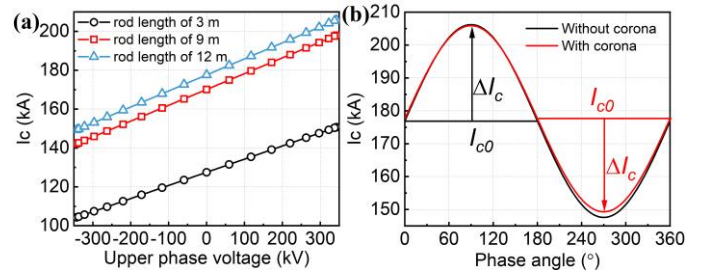$$I_c = \Delta I_c (\sin x) + I_{c0} \tag{24}$$

Fig. 11. (a) I_c of the Y-shaped pylon with different phase voltage when ground rods are 3 m, 9 m, and 12 m. (b) I_c of the Y-shaped pylon with and without corona considering when ground rod length is 12 m.

Where ΔI_c is the amplitude of the curve, which is an index to represent the phase voltage impact on I_c. I_{c0} is the I_c value at the zero-crossing point of the phase voltage. The coefficients in (24) at different ground rod conditions are listed in Table VI. We can find that the effect of the phase voltage becomes larger along with the increase of the rod length. Meanwhile, the occurrence of the corona weakens the ΔI_c, but $\Delta I_c + I_{c0}$ for cable considering the corona effect is higher than the value without considering

the corona, which makes sure that the I_c with corona is always higher than the case without considering corona whenever the lightning hits the shield wire.

The corresponding backflash rate (BFR) is also calculated. The amplitude of the lightning current I follows lognormal distribution [18]:

$$f(I) = \frac{1}{0.484\sqrt{2\pi}I} e^{-\frac{1}{2}\left(\frac{\ln\frac{I}{31.1}}{0.484}\right)^2} \quad (25)$$

The BFR can be expressed as [18]:

$$BFR = 0.6N_L \int_{I_c}^{\infty} f(I)\mathrm{d}I \quad (26)$$

$$N_L = \frac{N_g}{10}(28h_t^{0.6} + W) \quad (27)$$

Where h_t is the pylon height (22.5 m), and W is the width of the pylon. N_g is the lightning flash density, which is recommended to 1.39 flashes/km²·year in Denmark. N_L is the estimated number of strokes to transmission lines per year per 100 km, which is 28.1 flashes/km·year in this case. For the 400 kV steel towers such as Eagle and Donau towers [17], with the 12-meter ground rods and the same soil conditions, the BFR values are 0.0272 and 0.00575 times/100km-year [17]. The BFR value 0.0027 times/100km-year for the 'Y' composite pylon is lower than the values of the traditional lattice tower. Thus, the Y-shaped pylon with cable as a down-lead has potential advantages in lightning protection performance. The investigation of the BFR of the composite pylon with cable down-lead under different soil conditions or in regions with very high return strike currents can be performed as further work to fully validate its lightning protection performance.

TABLE VI
LIGHTNING PERFORMANCE OF Y PYLON WITH DIFFERENT ROD LENGTHS

	Rod length	ΔI_c (kA)	I_{c0} (kA)	BFR (flashes/100km-year)
Non-corona	3 m	23.2	126.6	0.0328
	9 m	28.9	168.8	0.0041
	12 m	29.3	176.3	0.0028
Corona	3 m	22.4	127.5	0.0300
	9 m	27.9	170.1	0.0038
	12 m	28.3	177.6	0.0027

V. CONCLUSIONS

In this paper, the electromagnetic model of the Y-shaped composite pylon with the cable as down-lead is built, and the impulse corona on the lightning performance is investigated. The following conclusions can be drawn:

(1) The multistory model can be used for the inclined cable down-lead modeling in PSCAD, and the inclined cable can be treated as a horizontal cable to calculate its surge impedance.

(2) With the high-frequency voltage stressed on a pair of coaxial cylinders, we found that the corona can increase the cable capacitance only at the rising edge. The rest of the time, the capacitance value is the natural capacitance of the cable.

(3) The impulse corona induced by lightning will reduce the cable impedance, but the corresponding effect on I_c is counteracted by the decreased surge traveling velocity.

(4) The presence of the corona around the cable can increase the mutual coupling effect and the capacitance between the cable down-lead and the phase conductors, which can slightly increase the lightning performance of the pylon.

(5) With the increase of the ground rod length, the I_c of the tower has greatly increased with the electrode rod from 3m to 9 m, and then slightly increases with the 12 m rod. With the cable as down-lead, the BFR of the composite pylon is much lower than the required values for the transmission lines.

In summary, the corona effect on the increase of I_c is limited, and the Y-shaped pylon with cable as a down-lead shows a promising application in power transmission from the perspective of lightning protection performance.

VI. REFERENCES

[1] Jahangiri T, Wang Q, Da Silva F F, and C. L. Bak, "Electrical Design of a 400 kV Composite Tower," Germany: Springer, 2020.

[2] E. Zorla, C. Ipbuker, V. Gulik, S. Kovaljov, and A. H. Tkaczyk "Optimization of basalt fiber in concrete composite for industrial application in Estonia," *Fresen. Environ Bull*, vol. 25, no. 1, pp.355-364, 2016.

[3] Q. Wang, C. L. Bak, F. F. da Silva, and E. Bystrup, "A state of the art review-methods to evaluate electrical performance of composite cross-arms and composite-based pylons," in *2016 IEEE Electri. Insul. Conf. (EIC)*, 2016, pp. 501-506.

[4] K. Yin, M. Ghomi, F. F. da Silva, C. L. Bak, H. Zhang, Q. Wang, and H. Skouboe, "Lightning performance and formula description of a Y-shaped composite pylon considering the effect of tower-footing impedance," in *2021 35th International Conference on Lightning Protection (ICLP) and XVI International Symposium on Lightning Protection (SIPDA)*, pp. 1-6.

[5] M. T. Correia de Barros, "Identification of the capacitance coefficients of multiphase transmission lines exhibiting corona under transient conditions," *IEEE Trans. Power Del.*, vol. 10, no. 3, pp. 1642-1648, Jul. 1995.

[6] C. de Jesus and M. T. Correia de Barros, "Modelling of corona dynamics for surge propagation studies," *IEEE Trans. Power Del.*, vol. 9, no. 3, pp. 1564-1569, Jul. 1994.

[7] C. A. Nucci, S. Guerrieri, M. T. Correia de Barros, and F. Rachidi, "Influence of corona on the voltages induced by nearby lightning on overhead distribution lines," *IEEE Trans. Power Del.*, vol. 15, no. 4, pp. 1265-1273, Oct. 2000.

[8] J. R. Riba, W. Larzelere, and J. Rickmann, "Voltage correction factors for air-insulated transmission lines operating in high altitude regions to limit corona activity: a review, " *Energies*, vol. 11, no. 7, p. 1908, Jul. 2018.

[9] P. Yutthagowith, T. H. Tran, Y. Baba, A. Ametani, and V. A. Rakov, "PEEC simulation of lightning over-voltage surge with corona discharges on the overhead wires," *Electr. Power Syst. Res.*, vol. 180, p. 106118, Jul. 2020.

[10] J. M. Li, Y. Zhang, Y. Wen, and L. Wen, "Improvement on the corona model of ultra high voltage alternating current transmission lines," in *2013 IEEE International Conference on Applied Superconductivity and Electromagnetic Devices*, pp. 69-75.

[11] M. T. C. de Barros and M. E. Almeida, "Computation of electromagnetic transients on nonuniform transmission lines," *IEEE Trans. Power Del.*, vol. 11, no. 2, pp. 1082-1091, Apr. 1996.

[12] H. Zhang, M. Ghomi, Q. Wang, F. F. da Silva, C. L. Bak, K. Yin, and H. Skouboe, "Comparison of Backflashover performance between a novel composite pylon and metallic towers," *Electr. Power Syst. Res.*, vol. 196, p. 107263, Jul. 2021.

[13] Q. Wang, T. Jahangiri, C. L. Bak, F. F. da Silva, and H. Skouboe, "Investigation on Shielding Failure of a Novel 400-kV Double-Circuit Composite Tower," *IEEE Trans. Power Del.*, vol. 33, no. 2, pp. 752-760, Apr. 2018.

[14] T. Jahangiri, Q. Wang, C. L. Bak, F. F. da Silva, and H. Skouboe, "Electric stress computations for designing a novel unibody composite cross-arm using finite element method," *IEEE Trans. Dielectr. Electr. Insul.*, vol. 24, no. 6, pp. 3567-3577, Dec. 2017.

[15] J. Li, Z. Peng, and X. Yang, "Potential calculation and grading ring design for ceramic insulators in 1000 kV UHV substations," *IEEE Trans. Dielectr. Electr. Insul.*, vol. 19, no. 2, pp. 723-732, Apr. 2012.

[16] M. Ishii, T. Kawamura, T. Kouno, E. Ohsaki, K. Shiokawa, K. Murotani, and T. Higuchi, "Multistory transmission tower model for lightning surge analysis," *IEEE Trans. Power Del.*, vol. 6, no. 3, pp. 1327-1335, Jul. 1991.

[17] K. Yin, M. Ghomi, H. Zhang, F. M. F. da Silva, C. L. Bak, Q. Wang, and H. Skouboe, "The Design and Optimization of the Down-Lead System for a Novel 400 kV Composite Pylon," *IEEE Trans. Power Del.* Accessed on: Jul. 25, 2022 [Online]. Available: https://ieeexplore.ieee.org/abstract/document/9839578

[18] A. R. Hileman, *Insulation coordination for power systems* (CRC Press, Boca Raton, Florida), 1999.

[19] J. A. Martinez-Velasco, ed., *Power system transients: parameter determination*. CRC Press, 2017.

[20] A. Deri, G. Tevan, A. Semlyen, and A. Castanheira, "The Complex Ground Return Plane a Simplified Model for Homogeneous and Multi-Layer Earth Return," *IEEE Trans. Power App. Syst.*, vol. PAS-100, no. 8, pp. 3686-3693, Aug. 1981.

[21] L. Grcev, "Modeling of Grounding Electrodes Under Lightning Currents," *IEEE Trans. Electromagn. Compat.*, vol. 51, no. 3, pp. 559-571, Aug. 2009.

[22] M. Ghomi, H. Zhang, C. L. Bak, F. F. da Silva, and K. Yin, " Integrated model of transmission tower surge impedance and multilayer grounding system based on full-wave approach," *Electr. Power Syst. Res.*, vol. 198, p. 107355, Sep. 2021.

[23] M. Nazari, R. Moini, S. Fortin, F. P. Dawalibi and F. Rachidi, "Impact of Frequency-Dependent Soil Models on Grounding System Performance for Direct and Indirect Lightning Strikes," *IEEE Trans. Electromagn. Compat.*, vol. 63, no. 1, pp. 134-144, Feb. 2021.

[24] CIGRE WG C4.23, "Procedures for estimating the lightning performance of transmission lines - New aspects," CIGRE Technical Brochure 839, Jun. 2021.

[25] K. Yin, G. Zhu, Y. Shi, H. Zhang, F. F. da Silva, C. L. Bak, and X. Chen, "Integrated model of transmission tower surge impedance and multilayer grounding system based on full-wave approach," *Electr. Power Syst. Res.*, vol. 217, p. 109154, Apr. 2023.

[26] E. Kuffel, W.S. Zaengl, J. Kuffel, High voltage engineering fundamentals (Second Edition), vol. IV. Oxford: Elsevier, 2000, p. 210.

[27] Erika Stracqualursi, Rodolfo Araneo, and Amedeo Andreotti. "The impact of different corona models on FD algorithms for the solution of multiconductor transmission lines equations, " *High Volt.*, vol. 6, no. 5, pp. 822–835, Sep. 2021.

[28] J. Cuarán, M. Becerra and F. Roman, "Lightning Attachment to UHV Power Transmission Lines: Effect of the Phase Voltage," *IEEE Trans. Power Del.*, vol. 34, no. 2, pp. 729-738, Apr. 2019.